J. Fluid Mech. (1969), *vol.* 35, *part* 1, *pp.* 77–96
Printed in Great Britain

Large-amplitude motions of a liquid–vapour interface in an accelerating container

By L. M. PERKO

Lockheed Palo Alto Research Laboratory, Palo Alto, California

(Received 24 August 1967 and in revised form 15 May 1968)

This paper considers the large-amplitude symmetric and asymmetric irrotational motion of an inviscid incompressible fluid with a liquid–vapour interface in an accelerating container of revolution. A combined analytical–numerical method which involves no linearizations in the hydrodynamical equations and applies to all but surface-tension dominated motions is used to compute a variety of such motions. One important aspect of this non-linear method is that it accurately determines the initial development of surface instabilities such as breakers near the wall of the container.

1. Introduction

This paper considers the dynamic behaviour of the liquid–vapour interface of an inviscid fluid in an accelerating cylindrical container. There have been several linearized analyses of this dynamical problem in recent years; e.g. Satterlee & Reynolds (1964), Fung (1965) and Bowman (1966). This last reference presents some large-amplitude motions predicted by the linearized analysis which offer good qualitative agreement with experimental results. The only large amplitude analysis that the author is familiar with besides the work of Moore & Perko (1965), hereafter referred to as M & P, and the work of Concus, Crane & Perko (1965), is that by Harlow & Welch (1965, 1966), who took viscosity into account, but not surface-tension effects. Their results for inviscid flow agree qualitatively very well with the M & P results with zero surface tension, and a comparison of their inviscid and viscous results indicates that viscosity tends to reduce the rate at which the velocity increases near the wall in reorientation motions.

The large-amplitude analysis of this paper generalizes the analysis of M & P to the asymmetric case in an arbitrary container of revolution and includes the constant contact angle boundary condition necessary to have a well-posed problem in the computation. The method is based on the expansion of the velocity potential in a series of harmonic functions with time-dependent coefficients. The time-dependent coefficients are determined numerically by an orthonormalizing computation in order to satisfy the required boundary conditions. Different sets of harmonic functions and various orthogonalizing computations have been used in the analysis. The results, including the development of a breaker at the wall in the computation of reorientation motions, are independent of the par-

ticular set of harmonic functions used. Surface tension is again included as a smoothing term in the computation as described in §3 and this is found to work well in all but motions dominated by surface tension.

One of the most interesting features of this work is that it lends some insight into the development of surface instabilities, i.e. the development of surface waves or breakers, in the context of a non-linear analysis. It was already seen in the work of M & P (cf. p. 314) that a Taylor instability was present in computations without surface tension and that surface tension had the effect of eliminating the development of surface waves of sufficiently small wavelength. It is pointed out in this paper that surface waves and breakers do develop in certain types of motion even with surface tension present and that the non-linear method of M & P (in the symmetric case and of this paper in the asymmetric case) accurately predicts the initial development of these surface instabilities. This type of information is not available from a linearized analysis. The initial development of these surface waves or breakers can be computed up to the point where the local curvature becomes so large that the surface-tension term in Bernoulli's equation dominates. This leads to numerical instabilities which cause the computation to stop. In order to compute the surface motion beyond the point at which surface waves or breakers begin to develop, a method of local smoothing is used which allows the global surface motion to be accurately computed at the expense of not being able to follow the local development of any surface waves or breakers that may develop. This method is useful only if the surface waves or breakers remain sufficiently localized. This is typically the case in reorientation motions, but is not always true in large-amplitude lateral sloshing. The results obtained by this method are found to be in excellent qualitative agreement with experimental results and with certain theoretical results of a qualitative nature as is pointed out in §5.

Sections 2 and 3 of this paper present the boundary-value problem and method of solution for the asymmetric problem in an arbitrary container of revolution including the constant contact-angle boundary condition. Some asymmetric results in which the contact angle is maintained nearly constant (if $\beta \neq 0$) are given in the latter part of §5. The reader who is familiar with the work of M & P and who is interested in the development of surface instabilities in the context of that non-linear analysis may proceed directly to §§4 and 5.

2. Problem formulation

Let $\mathbf{v}(r, \theta, z, t)$ be the velocity of a point (r, θ, z) in the fluid at time t. It is assumed that the flow is irrotational, i.e. that $\nabla \times \mathbf{v} = 0$ so that there exists a velocity potential $\phi(r, \theta, z, t)$ such that $\mathbf{v} = \nabla\phi$. The geometry is indicated in figure 1. Since the flow is assumed incompressible, the equation of continuity implies that $\nabla . \mathbf{v} = 0$ and hence that the velocity potential satisfies Laplace's equation interior to the fluid, i.e.

$$\phi_{rr} + \frac{1}{r}\phi_r + \frac{1}{r^2}\phi_{\theta\theta} + \phi_{zz} = 0 \tag{1}$$

for $G(r,z) < 0$, $0 < z < f(r,\theta,t)$, $0 \leqslant \theta \leqslant 2\pi$ and $t > 0$, where $G(r,z) = 0$ is the equation of the axisymmetric container and where $z = f(r,\theta,t)$ is the equation of the free surface. The normal derivative is assumed to be zero on the surface of the container; i.e.

$$\left.\frac{\partial\phi}{\partial n}\right|_{G(r,z)=0} = \left.\frac{\phi_r G_r + \phi_z G_z}{(G_r^2+G_z^2)^{\frac{1}{2}}}\right|_{G(r,z)=0} = 0 \tag{2}$$

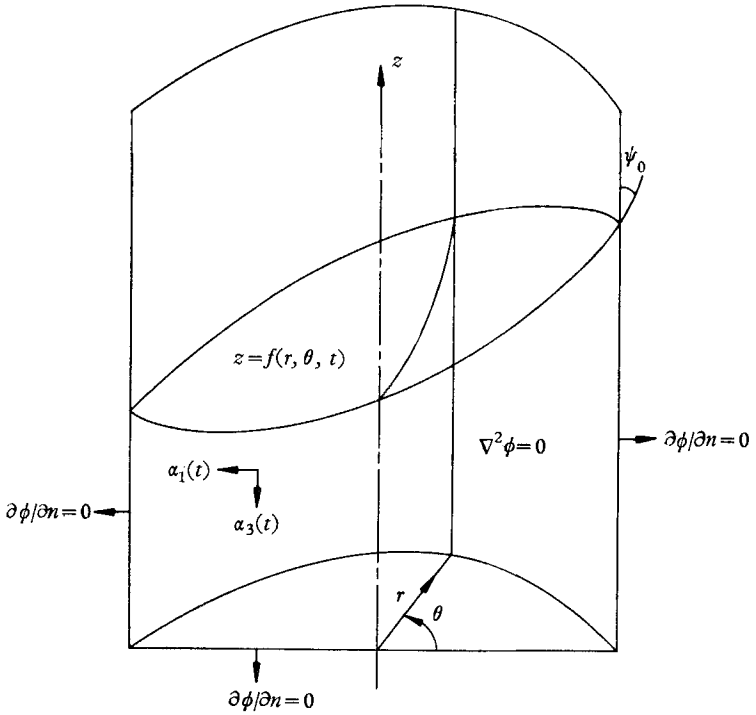

FIGURE 1. Container geometry and free surface.

for $0 \leqslant z \leqslant f(r,\theta,t)$, $0 \leqslant \theta \leqslant 2\pi$ and $t > 0$. As was previously indicated, $G(r,z) = 0$ is the equation of the axisymmetric container; e.g. for the flat-bottomed container of radius one shown in figure 1,

$$G(r,z) = \begin{cases} r-1 & \text{for} \quad r \geqslant 1, \\ -z & \text{for} \quad 0 \leqslant r < 1 \end{cases}$$

and

$$\left.\frac{\partial\phi}{\partial n}\right|_{G=0} = \begin{cases} \phi_r(1,\theta,z,t) & [0 \leqslant z \leqslant f(1,\theta,t)], \\ -\phi_z(r,\theta,0,t) & (0 \leqslant r < 1) \end{cases}$$

for $0 \leqslant \theta \leqslant 2\pi$ and $t \geqslant 0$.

The free surface boundary condition which follows from a first integral of Euler's equation for inviscid flow (Landau & Lifshitz 1959, p. 3) is known as Bernoulli's equation. It can be written in the form

$$\left.\begin{aligned} &\phi_t(r,\theta,z,t)|_{z=f(r,\theta,t)} = \Phi(r,\theta,t), \\ &\Phi(r,\theta,t) = \frac{1}{1+\beta}[\alpha_1(t) r\cos\theta + \alpha_2(t) r\sin\theta + \alpha_3(t)(f-H)] \\ &\qquad\qquad - \tfrac{1}{2}[\nabla\phi(r,\theta,f,t)]^2 + \frac{\beta}{1+\beta}\nabla.\left[\frac{\nabla f}{(1+|\nabla f|^2)^{\frac{1}{2}}}\right], \end{aligned}\right\} \tag{3}$$

where $f = f(r, \theta, t)$ describes the free surface. In (3), H is the volumetric average height and the dimensionless parameter.

$$\beta = \frac{\sigma}{\rho r_0^2 g} = \frac{1}{B},$$

where B is the axial Bond number. The last term in (3) is the expression for the mean curvature of the free surface, i.e. the surface tension term. It can be written out as

$$\nabla . \left[\frac{\nabla f}{(1 + |\nabla f|^2)^{\frac{1}{2}}} \right] = \frac{1}{r} \frac{\partial}{\partial r} \left[\frac{r f_r}{(1 + f_r^2 + r^{-2} f_\theta^2)^{\frac{1}{2}}} \right] + \frac{1}{r^2} \frac{\partial}{\partial \theta} \left[\frac{f_\theta}{(1 + f_r^2 + r^{-2} f_\theta^2)^{\frac{1}{2}}} \right]. \tag{4}$$

The co-ordinates in (1)–(3) have been normalized by dividing distance by r_0, time by $[r_0/g(1+\beta)]^{\frac{1}{2}}$ and the velocity potential by $[r_0^3 g(1+\beta)]^{\frac{1}{2}}$. Laplace's equation (1) and the boundary conditions (2) and (3) remain invariant under this normalization. The constants r_0 and g can be any distance and acceleration; however, in practice r_0 is conveniently taken as the maximum radius of the axisymmetric container and g is taken as the magnitude of the maximum acceleration on the container. $(\alpha_1(t)g, \alpha_2(t)g, \alpha_3(t)g)$ is the actual time varying acceleration on the container.

Associated with the boundary condition (3) is the boundary condition at the liquid–vapour–solid interface which geometrically requires the contact angle, ψ_0, to be maintained constant. It is expressed by the equation

$$-\frac{\nabla G . \nabla G_1}{|\nabla G| \, |\nabla G_1|} = \cos \psi_0, \quad (t \geqslant 0, \, 0 \leqslant \theta \leqslant 2\pi), \tag{5}$$

where as before $G(r, z) = 0$ describes the axisymmetric container surface and where $G_1(r, z, \theta, t) \equiv z - f(r, \theta, t) = 0$ describes the free surface. For example, if the container is a cylinder of radius one (in normalized co-ordinates), this condition reduces to

$$\frac{f_r(1, \theta, t)}{[1 + f_r^2(1, \theta, t) + f_\theta^2(1, \theta, t)]^{\frac{1}{2}}} = \cos \psi_0 \tag{6}$$

for $t \geqslant 0$, $0 \leqslant \theta \leqslant 2\pi$.

The remaining equation, which together with (3) relates the motion of the surface to the potential, follows from the definition of the velocity as

$$\mathbf{v} = d\mathbf{r}/dt,$$

where $\mathbf{r}(t)$ is a point in the fluid corresponding to (r, θ, z) at time t, on the surface $z = f(r, \theta, t)$. This equation can be written in component form as:

$$\frac{dr}{dt} = \phi_r, \quad r \frac{d\theta}{dt} = \frac{1}{r} \phi_\theta, \quad \frac{df}{dt} = \phi_z.$$

Using the fact that the total derivative

$$\frac{df}{dt} = f_t + f_r \frac{dr}{dt} + f_\theta \frac{d\theta}{dt},$$

these equations can be combined into the single first-order partial differential equation, the kinematic equation,

$$f_t = \phi_z - \phi_r f_r - \frac{1}{r^2}\phi_\theta f_\theta, \tag{7}$$

on $z = f(r, \theta, t)$, for $G(r, z) \leqslant 0$, $0 \leqslant \theta \leqslant 2\pi$, $t \geqslant 0$.

The remaining information necessary to complete the description of the mathematical model are the initial conditions at $t = 0$. These conditions can be given in the form of an initial free surface shape

$$f(r, \theta, 0) = f_0(r, \theta) \tag{8}$$

together with the initial velocity of the free surface

$$\left.\begin{aligned} u(r, \theta) &= \phi_r(r, \theta, f_0(r, \theta), 0), \\ v(r, \theta) &= \frac{1}{r}\phi_\theta(r, \theta, f_0(r, \theta), 0), \\ w(r, \theta) &= \phi_z(r, \theta, f_0(r, \theta), 0), \end{aligned}\right\} \tag{9}$$

for $G(r, z) \leqslant 0$, $0 \leqslant \theta \leqslant 2\pi$ or alternatively one can prescribe the initial free surface shape, $f_0(r, \theta)$, together with the initial velocity potential

$$\phi(r, \theta, z, 0) = \phi_0(r, \theta, z), \tag{10}$$

for $$G(r, z) \leqslant 0, \quad 0 \leqslant z \leqslant f_0(r, \theta) \quad 0 \leqslant \theta \leqslant 2\pi.$$

Laplace's equation (1) together with the boundary conditions (2), (3), (5) and (7) and the initial conditions (8) and (9) or (10) define the free surface boundary-value problem to be solved.

3. Method of solution

The method used to approximate the solution to the problem posed in the preceding section is the natural extension of the symmetric analysis of M & P to the asymmetric case. In brief, it is assumed that the velocity potential is represented in the form of an infinite series

$$\phi(r, \theta, z, t) \sim \sum_{n=0}^{\infty} c_n(t)\,\psi_n(r, \theta, z), \tag{11}$$

where the functions $\psi_n(r, \theta, z)$ satisfy Laplace's equation (1) and possibly some of the boundary conditions, e.g. (2). The time-dependent coefficients $c_n(t)$ are determined numerically by an orthonormalizing computation in order to satisfy those boundary conditions (2), (3), (5) and (7) which are not satisfied by $\psi_n(r, \theta, z)$. The description of the method will be limited to the case where the acceleration vector remains in a plane, e.g. $\alpha_2(t) = 0$, although it applies as well to the general case.

(i) *Separation of variables*

For a flat-bottomed cylindrical container, the velocity potential satisfying (1), (2) and $\phi_\theta(r, 0, z, t) = 0$ (since $\alpha_2(t) = 0$) has the representation, determined by separation of variables,

$$\phi(r, \theta, z, t) \sim \sum_{m,n=0}^{\infty} c_n^{(m)}(t) J_m(\lambda_n^{(m)} r) \cos m\theta \, \frac{\cosh(\lambda_n^{(m)} z)}{\cosh(\lambda_n^{(m)} H)}, \tag{12}$$

where $J'_m(\lambda_n^{(m)}) = 0$ determines the numbers $\lambda_n^{(m)}$, m, $n = 0, 1, 2, \ldots$. The time variation of the velocity potential $\phi(r, \theta, z, t)$ (i.e. of the coefficients $c_n^{(m)}(t)$) is determined by requiring that the representation (12) satisfy the boundary condition (3); i.e. that

$$\sum_{m,n=0}^{\infty} \frac{dc_n^{(m)}(t)}{dt} F_n^{(m)}(r, \theta, t) \sim \Phi(r, \theta, t), \tag{13}$$

where

$$F_n^{(m)}(r, \theta, t) = J_m(\lambda_n^{(m)} r) \cos m\theta \frac{\cosh [\lambda_n^{(m)} f(r, \theta, t)]}{\cosh (\lambda_n^{(m)} H)}. \tag{14}$$

This condition can be approximately satisfied by determining the first few coefficients $c_n^{(m)}(t)$ numerically by an orthonormalizing computation over the free surface; cf. Davis & Rabinowitz (1961, pp. 56–83) for a general description of orthonormalizing methods. Actually, a much less ambitious computation was carried out. Only the first few coefficients of the fundamental $c_n^{(0)}(t)$, $n = 0, \ldots, N_0$ and first harmonic $c_n^{(1)}(t)$, $n = 0, \ldots, N_1$ modes were determined. This was accomplished by following the motion of the free surface and orthonormalization on the $(\theta = \pm \frac{1}{2}\pi)$-plane and on the $(\theta = 0, \pi)$-plane. That is, the derivatives of $c_n^{(0)}(t)$ are determined from Bernoulli's equation (13), on the $(\pm \frac{1}{2}\pi)$-plane assuming that the effect of the second and higher harmonics remains small; i.e. assuming

$$\frac{dc_n^{(2)}(t)}{dt} \approx 0, \quad \frac{dc_n^{(3)}(t)}{dt} \approx 0, \quad \ldots.$$

With this assumption, it follows from (13) that

$$\sum_{n=0}^{N_0} \frac{dc_n^{(0)}(t)}{dt} F_n^{(0)}(r, \pm \tfrac{1}{2}\pi, t) \approx \Phi(r, \pm \tfrac{1}{2}\pi, t).$$

The derivatives of the $c_n^{(0)}(t)$ are then determined from this equation by the orthonormalization technique used in M & P. The function $\Phi(r, \pm \frac{1}{2}\pi, t)$ is defined by (3) with $\alpha_2(t) = 0$ and $\theta = \pm \frac{1}{2}\pi$. Having determined the derivatives of $c_n^{(0)}(t)$, the derivatives of the coefficients of the first harmonic, $c_n^{(1)}(t)$, $n = 0, \ldots, N_1$, are then determined from Bernoulli's equation on the $(0, \pi)$-plane assuming that the second and higher harmonics remain small; i.e. from

$$\sum_{n=0}^{N_1} \frac{dc_n^{(1)}}{dt} F_n^{(1)}(r, \overset{0}{\pi}, t) \approx \Phi(r, \overset{0}{\pi}, t) - \sum_{n=0}^{N_0} \frac{dc_n^{(0)}(t)}{dt} F_n^{(0)}(r, \overset{0}{\pi}, t),$$

using the orthonomalization scheme used in M & P. Having determined these derivatives at time t leads to the predicted values of the first few coefficients

$$c_n^{(m)}(t + \Delta t) \approx c_n^{(m)}(t) + \frac{dc_n^{(m)}}{dt}(t) \Delta t$$

for $m = 0, 1$ and hence to an approximation for the predicted velocity potential throughout the entire fluid from (12). The predicted surface shape at $t + \Delta t$ follows from the kinematic equation (7) as

$$f(r, \theta, t + \Delta t) \approx f(r, \theta, t) + f_t(r, \theta, t) \Delta t = f(r, \theta, t) + [\phi_z - f_r \phi_r - (1/r^2) \phi_\theta f_\theta](r, \theta, t) \Delta t. \tag{15}$$

Having computed the predicted coefficients and surface shape, one then proceeds to the correction step of the modified Euler method to move ahead one increment of time. The time-dependent coefficients $c_n^{(0)}(t)$, $n = 0, \ldots, N_0$ and $c_n^{(1)}(t)$, $n = 0, \ldots, N_1$ and the motion of the free surface $f(r, \theta, t)$ (based on the fundamental and first harmonic of the velocity potential) are determined in this way. The computation scheme is outlined in figure 2.

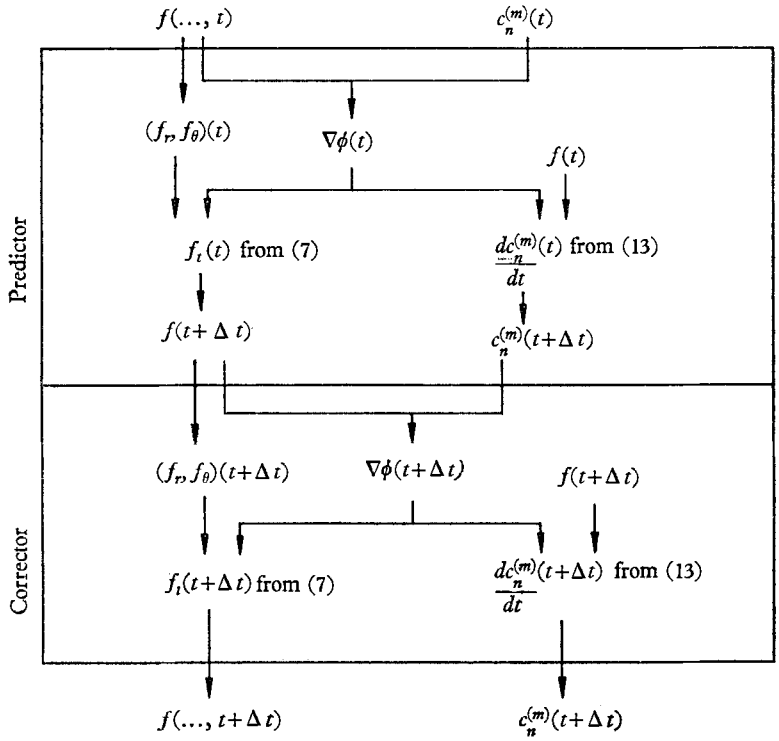

FIGURE 2. Computation scheme for the separation of variables approach.

The above description is for a fixed r-mesh. If f_r becomes unbounded, it is necessary to use a variable r-mesh; i.e. to follow the r-characteristics as was done in M & P; i.e. we let

$$r(t+\Delta t) \approx r(t) + \phi_r(\ldots, t)\,\Delta t$$

and

$$f(r(t+\Delta t), \theta, t+\Delta t) \approx f(r(t), \theta, t) + \left[\phi_z - \frac{1}{r^2}\phi_\theta f_\theta\right](\ldots, t)\,\Delta t$$

in the predictor step, etc.

The mean curvature of the surface $f(r, \theta, t)$, i.e. the surface tension term in Bernoulli's equation (3), is computed by finite differencing based on the values of $f(r, \theta, t)$ on the θ = constant planes and neighbouring planes. Note that a knowledge of the velocity potential throughout the entire fluid allows one to follow the motion of any point in the fluid and in particular any point on the surface. The boundary condition (6) is incorporated into the surface-tension computation at the wall; i.e. it is used in the finite differencing in order to compute the mean curva-

ture at the wall. The effect of incorporating this boundary condition into the computation is to maintain the contact angle very nearly constant. This method of including surface tension in the computation has a stabilizing effect on the surface motion in the sense that it eliminates the growth of any small wavelength surface waves which may appear due to round off error, etc. However, this method of including surface tension does not yield accurate results in the computation of surface-tension-dominated motions, i.e. we must require that

$$\left|\frac{\boldsymbol{\alpha}(t)\cdot\mathbf{r}(t)}{1+\beta}-\tfrac{1}{2}(\nabla\phi)^2\right| \gg \left|\frac{\beta}{1+\beta}\nabla\cdot\left[\frac{\nabla f}{(1+|\nabla f|^2)^{\frac{1}{2}}}\right]\right| \tag{16}$$

be satisfied in the right-hand side of Bernoulli's equation in order to obtain accurate results by this method. It has not been possible to determine the validity of the assumption that the effect of the higher harmonics remains small. This effect can be determined by going to a surface orthonormalization.

(ii) *An alternative harmonic expansion*

A second representation of the form (11) was utilized in order to study the dependence of the method on the particular set of harmonic functions that was used. It was of special interest to see what effect a change in the set of harmonic functions had on the development of the instability encountered in reorientation motions. The representation (11) for the case $\alpha_2(t) = 0$ was assumed in the form of an expansion in terms of harmonic functions

$$\phi(r,\theta,z,t) \sim \sum_{n,m=0}^{\infty} c_n^{(m)}(t)\,\psi_n^{(m)}(r,\theta,z),$$

where the functions

$$\psi_n^{(m)}(r,z,\theta) = \left(\frac{r}{2}\right)^m \sum_{k=0}^{[\frac{1}{2}n]} \frac{(-1)^k z^{n-2k}(\frac{1}{2}r)^{2k}}{(n-2k)!\,k!\,(k+m)!}\cos m\theta$$

satisfy Laplace's equation (1). This approach can be applied to the computation of asymmetric motions in arbitrary containers of revolution (e.g. hemispherical bottomed tanks) in which case the coefficients $c_n^{(m)}(t)$ are chosen to satisfy the zero normal derivative boundary condition on the container wall (2) as well as Bernoulli's equation (3), on the free surface. The method in brief is first to obtain the predicted potential function $\phi(r,\theta,z,t+\Delta t)$ on the surface from a knowledge of the total derivative of ϕ at time t given by

$$\frac{d\phi}{dt}(r,\theta,z,t)|_{z=f(r,\theta,z,t)} = \frac{\partial\phi}{\partial t}(r,\theta,z,t)|_{z=f(r,\theta\ t)} + (\nabla\phi)^2|_{z=f(r,\theta,t)}(r,\theta,z,t),$$

where ϕ_t is obtained from Bernoulli's equation at time t and the velocities which determine $(\nabla\phi)^2$ on the surface are known at time t. In this way, a mixed boundary-value problem, i.e. $\partial\phi/\partial n = 0$ on the container surface and ϕ prescribed on the free surface, is obtained for the potential ϕ at time $t+\Delta t$. The predicted coefficients $c_n^{(m)}(t+\Delta t)$ are then obtained by an orthonormalizing computation over the entire free surface and container surface. The computation scheme is outlined in figure 3. This scheme has only been implemented for the symmetric case (in which case the orthonormalization is over a curve rather than a surface).

The results of this computation for the symmetric case with a flat-bottomed container geometry were found to agree with the original results of M & P based on the separation of variables approach, including the development of breakers near the wall in the case of reorientation motions. Thus, the results of this method

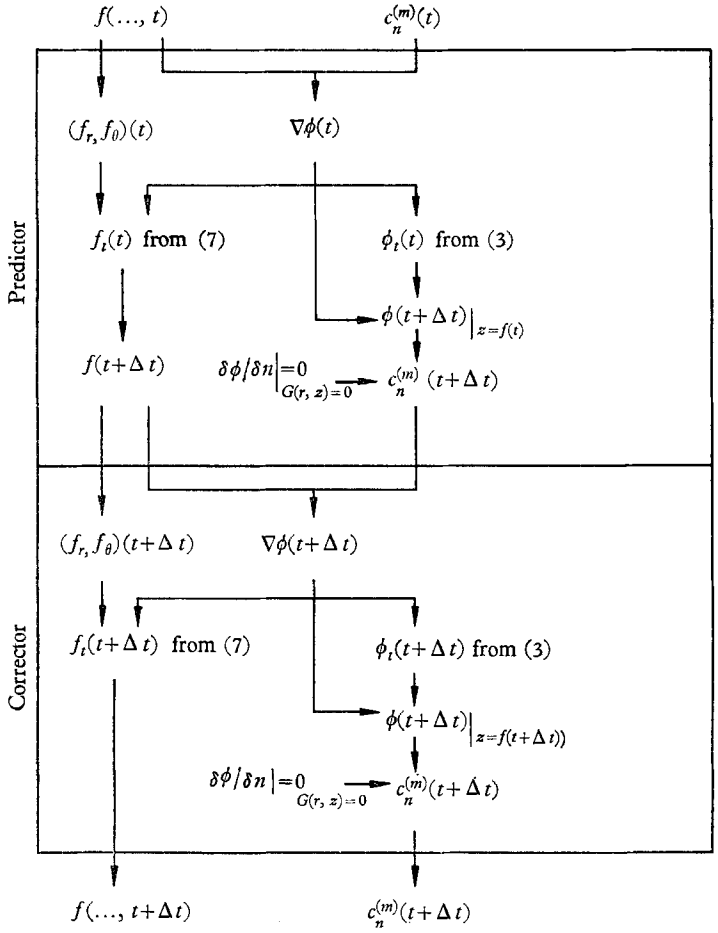

FIGURE 3. Computation scheme for the harmonic polynomials approach.

appear to be independent of the particular set of functions used in the representation of the velocity potential (provided that a sufficiently large number of these functions are used in the computation). The orthonormalization used in M & P did not work well for this computation. An orthonormalizing computation in which the functions are orthogonalized in an optimum order had to be used; cf. Householder (1958) and also Bussinger & Golub (1965).

(iii) *Expansion of the free surface displacement*

A second variation of the method outlined in § 3 (i) was employed to test the permanence of the results with a variation in method and to see what effect this variation might have on the development of the instability in reorientation

motions. The method is similar to the method originated by Penny & Price (1952) in their study of two-dimensional surface waves in which the free surface displacement as well as the velocity potential are expanded in a Fourier–Bessel series; i.e. we assume an expansion for the velocity potential $\phi(r, \theta, z, t)$ in the form given in (12) and an expansion for the free surface in the form

$$f(r, \theta, t) \sim f_0(r, \theta) + \sum_{m,n=0}^{\infty} b_n^{(m)}(t) J_m(\lambda_n^{(m)} r) \cos m\theta.$$

The time variation of the coefficients $b^{(m)}(t)$ is determined (in conjunction with determining the coefficients $c_n^{(m)}(t)$) as described in § 3 (i) by requiring the kinematic equation (7) to be satisfied, i.e. from

$$\sum_{m,n=0}^{\infty} \frac{db_n^{(m)}}{dt}(t) J_m(\lambda_n^{(m)} r) \cos m\theta \sim Q(r, \theta, t),$$

where

$$Q(r, \theta, t) = [\phi_z(r, \theta, z, t) - \phi_r(r, \theta, z, t) f_r(r, \theta, t) - r^{-2}\phi_\theta(r, \theta, z, t) f_\theta(r, \theta, t)]_{z=f(r,\theta,t)}.$$

This, as usual, is accomplished by an orthogonalizing computation. This gives the predicted values of $b_n^{(m)}(t + \Delta t)$, the modified Euler scheme being used to move ahead in time. This was implemented on the computer in the symmetric case and it was found that this approach agreed with the results obtained from the original approach, including the development of the breaker near the wall in reorientation motions.

(iv) *Non-zero initial velocity*

Starting the computation with non-zero velocity can be achieved in two ways: by specifying the velocity of the initial surface as in (9); or by specifying an initial non-zero velocity potential (10); i.e. by specifying one or more non-zero coefficients in the representation (11). The former of these two methods will be discussed in the case of the representation (12) since it may not be evident to the reader how to determine the initial coefficients $c_n^{(m)}(0)$ when the initial velocity of the free surface is prescribed. Given the initial velocity $\mathbf{v}(r, \theta) = (u(r, \theta), v(r, \theta), w(r, \theta))$, the coefficients $c_n^{(m)}(0)$ are determined by an orthonormalizing computation as follows. Suppose that

$$\phi(r, z, \theta, 0)|_{z=f_0(r,\theta)} \sim \sum_{m,n=0}^{\infty} c_n^{(m)}(0) F_n^{(m)}(r, \theta, 0),$$

where the functions $F_n^{(m)}(r, \theta, t)$ are defined in (14). The problem is then to determine the $c_n^{(m)}(0)$ to satisfy

$$\sum_{m,n=0}^{\infty} \lambda_n^{(m)} c_n^{(m)}(0) \mathbf{F}_n^{(m)}(r, \theta) \sim \mathbf{v}(r, \theta),$$

where the vector valued function $\mathbf{F}_n^{(m)}(r, \theta)$ can be written in component form as

$$\mathbf{F}_n^{(m)}(r, \theta) = \frac{1}{\cosh(\lambda_n^{(m)} H)} \begin{pmatrix} J_m'(\lambda_n^{(m)} r) \cosh[\lambda_n^{(m)} f_0(r, \theta)] \cos m\theta \\ \dfrac{-m}{\lambda_n^{(m)}} J_m(\lambda_n^{(m)} r) \cosh[\lambda_n^{(m)} f_0(r, \theta)] \sin m\theta \\ J_m(\lambda_n^{(m)} r) \sinh[\lambda_n^{(m)} f_0(r, \theta)] \cos m\theta \end{pmatrix}.$$

This can be accomplished by orthonormalizing the set of functions $\mathbf{F}_n^{(m)}(r, \theta)$ with respect to the inner product

$$(\mathbf{F}_n^{(m)}, \mathbf{F}_l^{(k)}) = \frac{1}{2\pi}\int_0^{2\pi}\int_0^1 \mathbf{F}_n^{(m)}(r,\theta).\mathbf{F}_l^{(k)}(r,\theta) r\,dr\,d\theta,$$

the dot denoting the usual vector inner product. This has been implemented in the symmetric case (i.e. $v(r, \theta) = 0$) and by reading in coefficients $c_n^{(0)}(0)$, $n = 1$, ..., 7 computing the initial velocities $u(r, \theta)$ and $w(r, \theta)$ and then using the technique described above to recompute the coefficients $c_n^{(0)}(0)$, $n = 1, \ldots, 7$, the computation being carried out in single precision, it was found that the computed coefficients agreed with the original coefficients to within an accuracy of $O(10^{-7})$.

4. Surface instabilities

It was pointed out by Taylor (1950) in a linearized analysis neglecting surface tension and viscosity that when a liquid surface is accelerated in a direction perpendicular to the surface with the acceleration vector directed from the more dense to the less dense fluid, the liquid surface becomes unstable. Furthermore, Taylor showed that the smaller the wavelength of the surface wave, the faster it grows, i.e. the rate of growth is proportional to $\lambda^{-\frac{1}{2}}$, where λ is the wavelength. This effect is referred to as the Taylor instability. These results were found to be in agreement with experimental results of Lewis (1950). When the acceleration vector is directed in this manner, we will refer to the surface as undergoing an upward acceleration. This type of Taylor instability was observed in the numerical results of M & P based on a non-linear analysis; cf. figures 2, 3 and 7, where $\beta = 0$. It was pointed out by Bellman & Pennington (1954) in a linearized analysis that surface tension removes the Taylor instability for sufficiently small wavelengths (relative to the surface tension parameter β). This was also observed in the non-linear work of M & P (1965); cf. figures 5 and 8.

Thus, due to the stabilizing influence of the surface tension, we were able to compute smooth surface motions which would otherwise experience surface splashing as a result of the Taylor instability. However, surface tension does not eliminate the development of surface splashes or surface breakers of sufficiently large wavelength (relative to β) as is evidenced by the experimental results of Lewis (1950), Abramson, Chu & Kana (1966) and figures 8 and 9, plate 1, of this report. As was pointed out in §3, the method of this paper is not applicable to the computation of surface tension dominated motions where (16) is not satisfied. Thus, once a splash or breaker has developed to the point where the mean curvature is very large, (16) will fail to be satisfied (even if $0 < \beta \ll 1$) and the computation will not be valid beyond this point. A numerical instability develops at this point and causes the computation to halt within a few iterations. However, up to this point the computation gives an accurate account of the surface motion. Thus, it is possible by this method to determine the time at which a surface splash or breaker begins to develop in the actual motion and to determine the initial development of the splash or breaker. These results are in good agreement with experimental results as is pointed out in the next section.

5. Numerical results

In the first part of this section we present some results for symmetric motions which: show the effect of including the constant contact angle boundary condition in the computation for $\beta \neq 0$; show that in reorientation motions with small β of order 10^{-2} breakers near the wall of the container of small wavelength $\lambda \approx 0{\cdot}07$ are not eliminated by surface tension and that the initial development of these breakers is accurately determined by this method; and show that in reorientation motions, local smoothing of the breakers near the wall allows one to compute the motion of the fluid from one end of the container to the other.

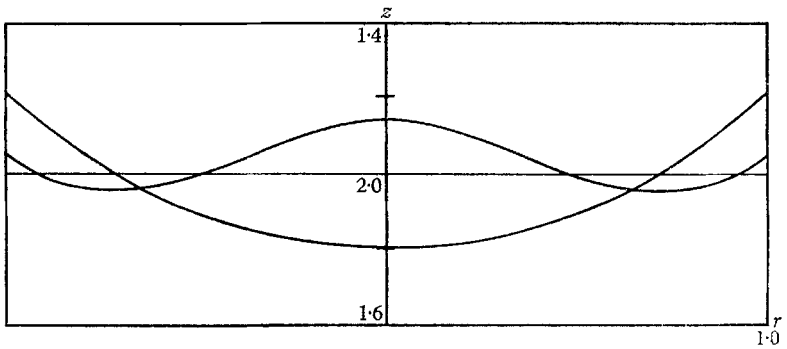

FIGURE 4. Symmetric oscillation envelope with $\alpha_1 = 0, \alpha_3 = -1{\cdot}0, \beta = 0{\cdot}05$ and $\psi_0 = 45°$.

The second part of this section gives some results for asymmetric motions based on the fundamental and first harmonic in the velocity potential as described in §3. It is shown that sustained transverse sloshing motions can be computed by this method and that the method accurately determines the initial development of a large amplitude surface wave of wavelength $\lambda \approx 0{\cdot}35$ excited by pure first-mode sloshing. These and other asymmetric results indicate that higher harmonics in the velocity potential have a secondary effect in the computation.

First of all, we note that including the boundary condition (6) in the computation as described in §3 results in a motion during which contact angle remains effectively constant. An example of this is shown in figure 4. This figure shows the envelope of an oscillatory motion which is basically the same as that shown in figure 8 of M & P except that the contact angle now remains constant. The velocity envelope for this motion, i.e. the velocity at the wall and at the centre, is shown in figure 5. All intermediate velocities lie between these two curves. The velocities return to zero and the surface to its initial shape (to within five-place accuracy when the computation is carried out in single precision) after an interval of normalized time $T \cong 2{\cdot}6$. Thus the resulting motion is an oscillatory motion with period T. As was pointed out in §4, surface tension removes the Taylor instability (which is present for $\beta = 0$ as seen in M & P, figure 7) on that part of the surface which is accelerating upward and allows the computation of a smooth oscillatory surface motion with contant contact angle by the method of §3.

We next consider a reorientation motion in which a breaker develops on the surface near the wall of the container, both in the computed motion and in the actual reorientation motion observed at the Lockheed drop-tower facility. The

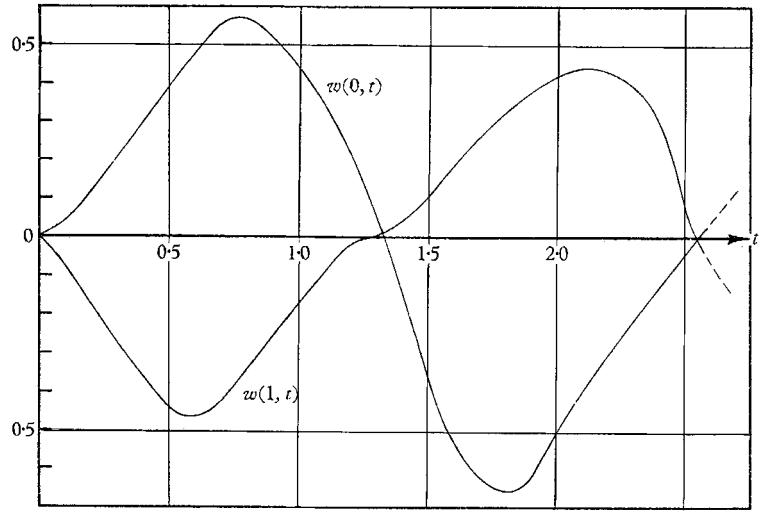

FIGURE 5. Vertical velocity envelope for the symmetric oscillatory motion of figure 4.

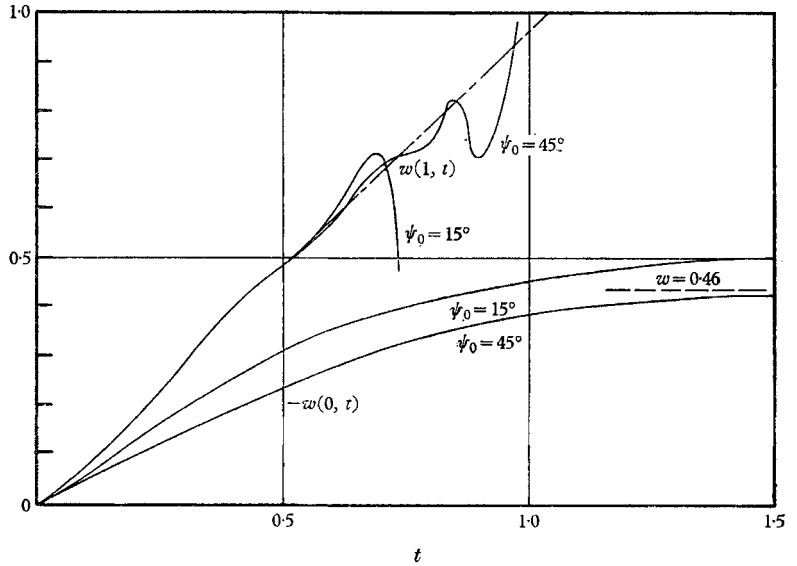

FIGURE 6. Vertical velocity envelope for a symmetric reorientation motion with $\alpha_1 = 0$, $\alpha_3 = 1{\cdot}0$, $\beta = 0{\cdot}00384$ and contact angles $\psi_0 = 15°$ and $\psi_0 = 45°$.

velocity profile for such a motion including surface tension is shown in figure 6. We see that at about $t = 0{\cdot}7$ (for both 15° and 45° contact angles) an oscillation in the velocity at (and near) the wall begins to develop. This corresponds to the development of a breaker near the wall similar to that shown in figure 3 of M & P even with surface tension present. It was observed in M & P, figure 5,

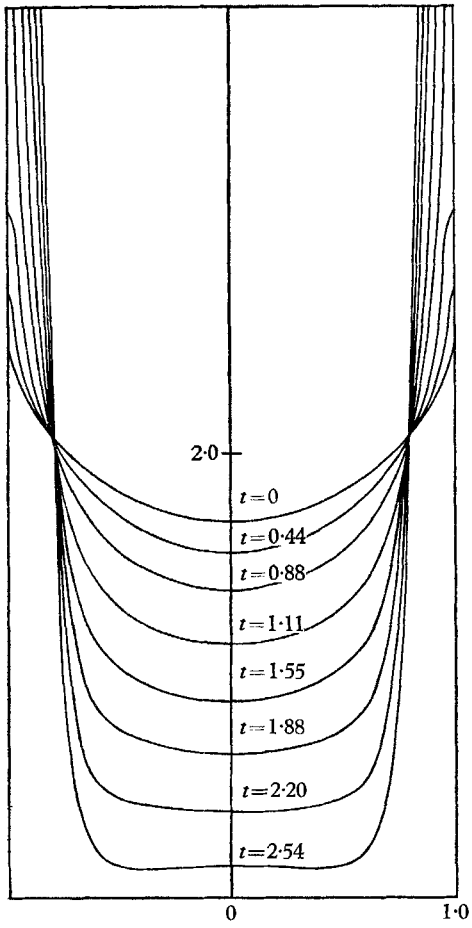

FIGURE 7

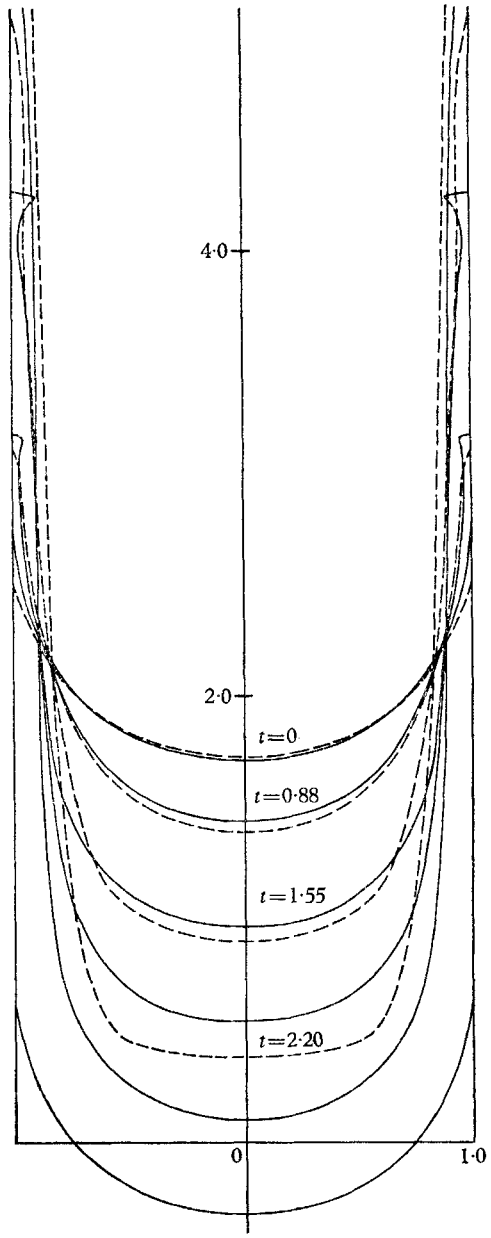

FIGURE 8

FIGURE 7. Symmetric reorientation with local smoothing near the wall for $\alpha_1 = 0$, $\alpha_3 = 1{\cdot}0$, $\beta = 0{\cdot}00384$ and $\psi_0 = 15°$.

FIGURE 8. Comparison of experimental and numerical results for symmetric reorientation with $\alpha_1 = 0$, $\alpha_3 = +1$, $\beta = 0{\cdot}00384$. The solid curves illustrate the experimental results which are for a hemispherical bottomed 6·96 cm diameter container and $\psi_0 = 0°$ and the dashed curves are the results of figure 7.

that using a variable time step (reduced at each step to keep the growth of the surface tension term in Bernoulli's equation less than some given bound) did result in a smooth motion with no apparent development of breakers for β sufficiently large. However, in that computation the size of the time step went to zero in the computation as $t \to t_1 \cong 0{\cdot}75$. With a knowledge that breakers develop near the wall in the actual fluid motion, it is evident that the computation points out this fact but is unable to continue because the condition (16) is no longer satisfied near the wall. The actual time at which the breakers begin to develop in the experimental results is difficult to pin-point from the movies taken, but it is somewhere in the range $0{\cdot}7 \leqslant t \leqslant 0{\cdot}8$, and the breaker is well developed by the time $t = 0{\cdot}88$ as can be seen in figure 8. The solid curves in figure 8 show a reorientation motion (for the parameters listed there) obtained from movies taken at the Lockheed drop-tower facility. For a description of the experimental apparatus used, cf. Satterlee *et al.* (1967). By the time $t = 1{\cdot}55$ a sharp spike has developed on the surface near the wall as is depicted in figure 8 and as can be seen in the photograph in figure 9, plate 1, which is an enlargement of the movie frame corresponding to $t = 1{\cdot}55$. The computational results thus indicate quite accurately the time at which a breaker begins to develop ($t \cong 0{\cdot}7$ independent of contact angle) and give some indication of the initial development of the breaker (e.g. in figure 3 of M & P all but the last two surface shapes probably give an accurate representation of the surface motion since (16) is satisfied up to that point). In looking at the velocity envelope for this motion up to the point at which a breaker begins to develop at the wall, one sees that the motion at the wall is approximately that of a free falling particle, $w(1,t) \cong t$, and the velocity at the centre $w(0,t)$ is approximately approaching the theoretical velocity of a bubble rising in an infinite fluid, $w = 0{\cdot}46$. Encouraged by the good quality of these results, it was natural to look for a way to extend the computation of the global motion beyond the point at which a breaker begins to develop at the wall without asking for a detailed description of the breaker development as the fluid moves along the wall. (The experimental results indicate that the development of the breakers is an unstable process and would thus require an extremely sensitive method to be able to compute this development. This is beyond the scope of this analysis.) A method of local smoothing was used to eliminate the development of breakers at the wall. This resulted in the smooth reorientation motion shown in figure 7, which is in good qualitative agreement with experimental results as shown in figure 8. The local smoothing technique simply extrapolates the velocity in the region where a large curvature begins to develop and thereby eliminates the large amplitude oscillations which develop in the vertical component of the velocity in these regions. The computation over the remainder of the surface then proceeds without modification. For the reorientation motion of figure 7, the velocity extrapolation resulted in the dashed straight line curve for the vertical velocity at the wall shown in figure 6 (and a similar velocity extrapolation for points near the wall $0{\cdot}93 \leqslant r \leqslant 1{\cdot}0$) and in the computed velocity at the centre shown in figure 6 (and at the remaining points $0 \leqslant r \leqslant 0{\cdot}93$). The bottom of the container has begun to influence the shape of the surface as is seen in figure 7, but has little effect on the velocity at the centre

until the surface gets very close to the bottom. These results are compared with similar experimental results obtained at the Lockheed drop-tower facility for a reorientation motion. The comparison is shown in figure 8 and is seen to be very good over a substantial part of the motion. The main difference in the experi-

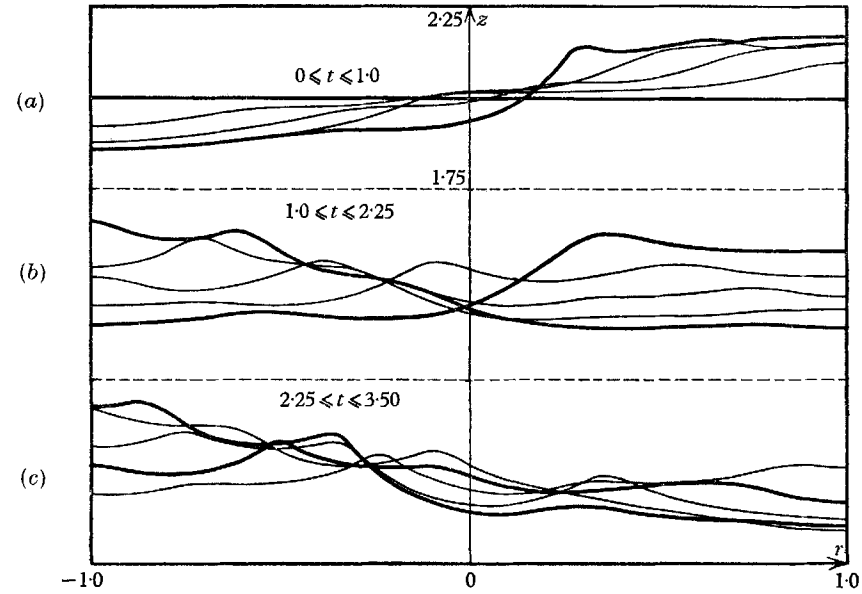

FIGURE 10. Transverse sloshing with $\alpha_1 = 4{\cdot}0$ for $0 \leqslant t \leqslant 0{\cdot}05$, $\alpha_1 = 0$ for $t > 0{\cdot}05$, $\alpha_3 = -2{\cdot}0$, $\beta = 0{\cdot}04$, $\psi_0 = 90°$.

mental and numerical results (beside the obvious effect of the flat-bottomed container on the numerical results) is that the velocity at the wall in the experimental results grows at a rate of approximately 0·7 (in the normalized coordinates) as compared with the rate of approximately 1·0 in the numerical work. The results of Harlow & Welch (1966) indicate that viscosity has exactly this sort of effect on the velocity of the fluid near the wall and would most likely account for this discrepancy in the rate of growth of the velocity near the wall.

We next discuss some of the results obtained from the asymmetric computation based on the fundamental and first harmonic in the velocity potential. Figure 10 shows the effect of a transverse impulse on a fluid making a 90° contact angle with the wall and initially at rest. The result is a back-and-forth transverse sloshing motion. After an impulse from the right has been applied to the container, a mound of fluid builds up on the right and a valley on the left, figure 10*a*. This is followed by a sloshing from right to left with the mound of fluid travelling across the container in the form of a travelling wave. This results in a mound of fluid on the left and a valley on the right, figure 10*b*. This is followed by a sloshing of the fluid in the opposite direction, figure 10*c*, etc. The impulse is described by

$$\alpha_1(t) = \begin{cases} 4{\cdot}0 & \text{for} \quad 0 \leqslant t \leqslant 0{\cdot}05, \\ 0 & \text{for} \quad t > 0{\cdot}05, \end{cases}$$

in figure 10. However, it was found that exactly the same results were obtained for any high initial transverse acceleration level (say $\alpha_1(0) \geqslant 1{\cdot}0$) provided the total impulse $\int_0^\infty \alpha_1(t)\,dt$ remained constant.

We next look at a pure first mode lateral slosh obtained by setting $c_1^{(1)}(0) = 0{\cdot}1$ and the other coefficients initially equal to zero in the expansion of the velocity potential (12). The results for an initially flat surface with $\psi_0 = 90°$ are shown in

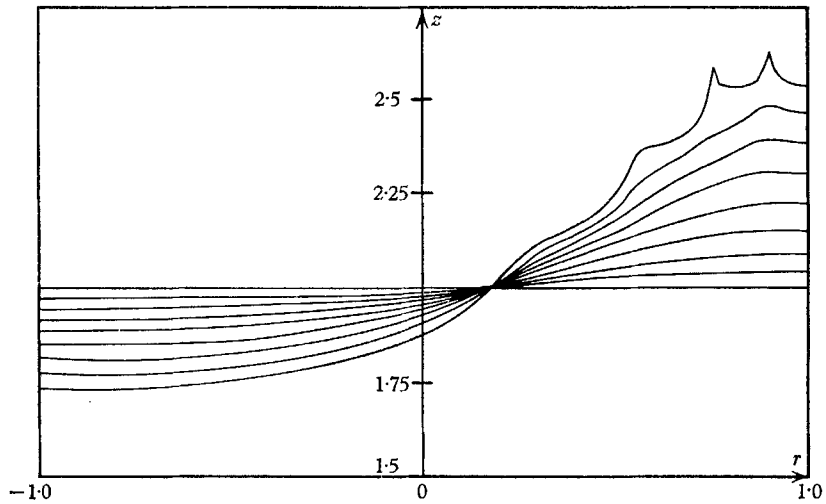

FIGURE 11. First-mode lateral sloshing with $\alpha_1 = \alpha_3 = \beta = 0$, $c_1^{(1)}(0) = 0{\cdot}1$, $\Delta t = 0{\cdot}5$ and $\psi_0 = 90°$.

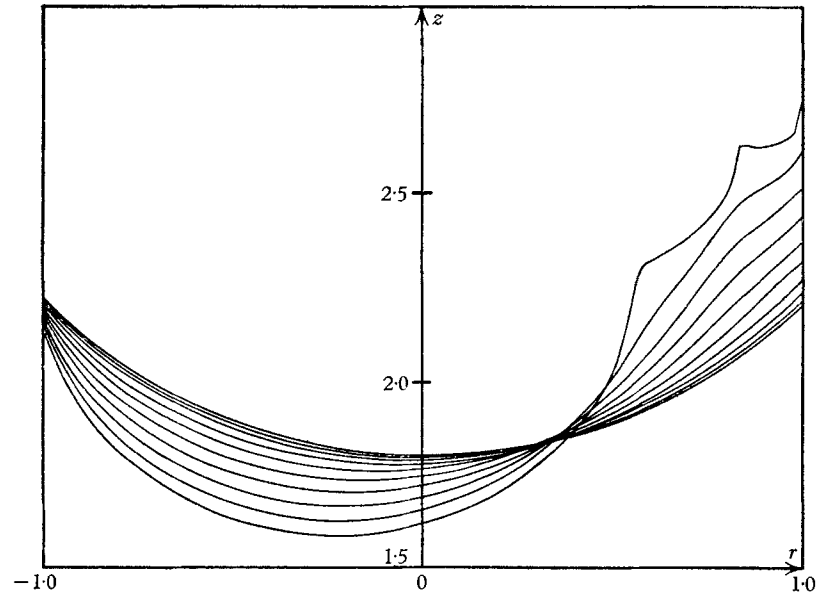

FIGURE 12. Asymmetric surface motion with $\alpha_1 = \alpha_3 = +1{\cdot}0$, $\beta = 0{\cdot}05$, $\Delta t = 0{\cdot}08$ and $\psi_0 = 45°$.

figure 11. One non-linear effect that is immediately seen is that the node occurs at approximately $r = 0{\cdot}2$ rather than at $r = 0$ as in the linear theory. The surface splashing that takes place on the part of the surface undergoing an upward acceleration illustrates the development of the Taylor instability in this region.

Since no surface tension is present ($\beta = 0$) in this case, the small wavelength surface waves which develop in the computation grow very fast and cause the computation to halt. Even with $\beta \neq 0$ in this type of motion a large-amplitude wave began to develop on the upper part of the surface when it reached a height of approximately one-half tank radius above the initial plane surface level. This took place in the r-interval $0{\cdot}55 \leqslant r \leqslant 1{\cdot}0$ as is indicated in figure 11. This agrees qualitatively very well with the experimental results of Abramson *et al.* (1966). Their figure 1 shows a well-developed large-amplitude breaking surface wave in the region $0{\cdot}55 \leqslant r \leqslant 1{\cdot}0$, $0{\cdot}5 \leqslant z - z_0 \leqslant 1{\cdot}0$ ($-\delta \leqslant \theta \leqslant \delta$, $\delta \ll 1$). Thus, it would again appear that the method of §3 is able to predict the time and initial development of a surface wave up to the point where (16) is no longer satisfied. The local smoothing technique described above could again be used to predict the gross motion beyond this point without accurately determining the surface splash. However, in this case, as the experimental results of Abramson *et al.* (1966) show, the wavelength of the surface wave, $\lambda = 0{\cdot}35 \pm 0{\cdot}05$, is not negligibly small as compared to the radius of the tank $R = 1{\cdot}0$ (in contrast to the reorientation motion of figure 8 where the breaker wavelength $\lambda \approx 0{\cdot}07 \ll 1$). Therefore, determining the gross surface motion in this case by smoothing over a relatively large local region would probably not give a good representation of the gross surface motion as it did in the case of the reorientation motion.

Figure 12 shows a large amplitude asymmetric reorientation in which the liquid is being poured out of a cylindrical container tilted at a 45° angle to the local horizon; i.e. $\alpha_1(t) = \alpha_3(t) = +1{\cdot}0$. The surface-tension parameter $F = 0{\cdot}05$ in this case and the contact angle is maintained very nearly constant at $\psi_0 = 45°$. The last surface shape shown does not satisfy (16) in the region $0{\cdot}5 \leqslant r \leqslant 1{\cdot}0$, $-\delta \leqslant \theta \leqslant \delta$, $\delta \ll 1$, and therefore does not represent a true surface shape. These results indicate that in this type of motion, a large-amplitude wave (with a relative large wavelength $\lambda \approx 0{\cdot}4$) will develop on the upper part of the surface, i.e. the surface tension does not eliminate the growth of large wavelength surface waves in this type of motion.

The last example is presented in order to emphasize the three-dimensional asymmetric aspect of the surface motion being computed. Figure 13 shows the motion that results when a liquid making a 45° contact angle with the wall initially in a zero-g environment is subject to an acceleration making a 45° angle with the axis of the container, i.e. $\alpha_1(t) = \alpha_3(t) = -1{\cdot}0$. The surface-tension parameter $\beta = 0$ in this example and thus the constant contact-angle boundary condition is not maintained. The computation terminates due to the development of a Taylor type instability on the part of the surface undergoing an upward acceleration.

This work was supported by the NASA Manned Spacecraft Center under Contract NAS 9-5174 and under the Lockheed Independent Research Program.

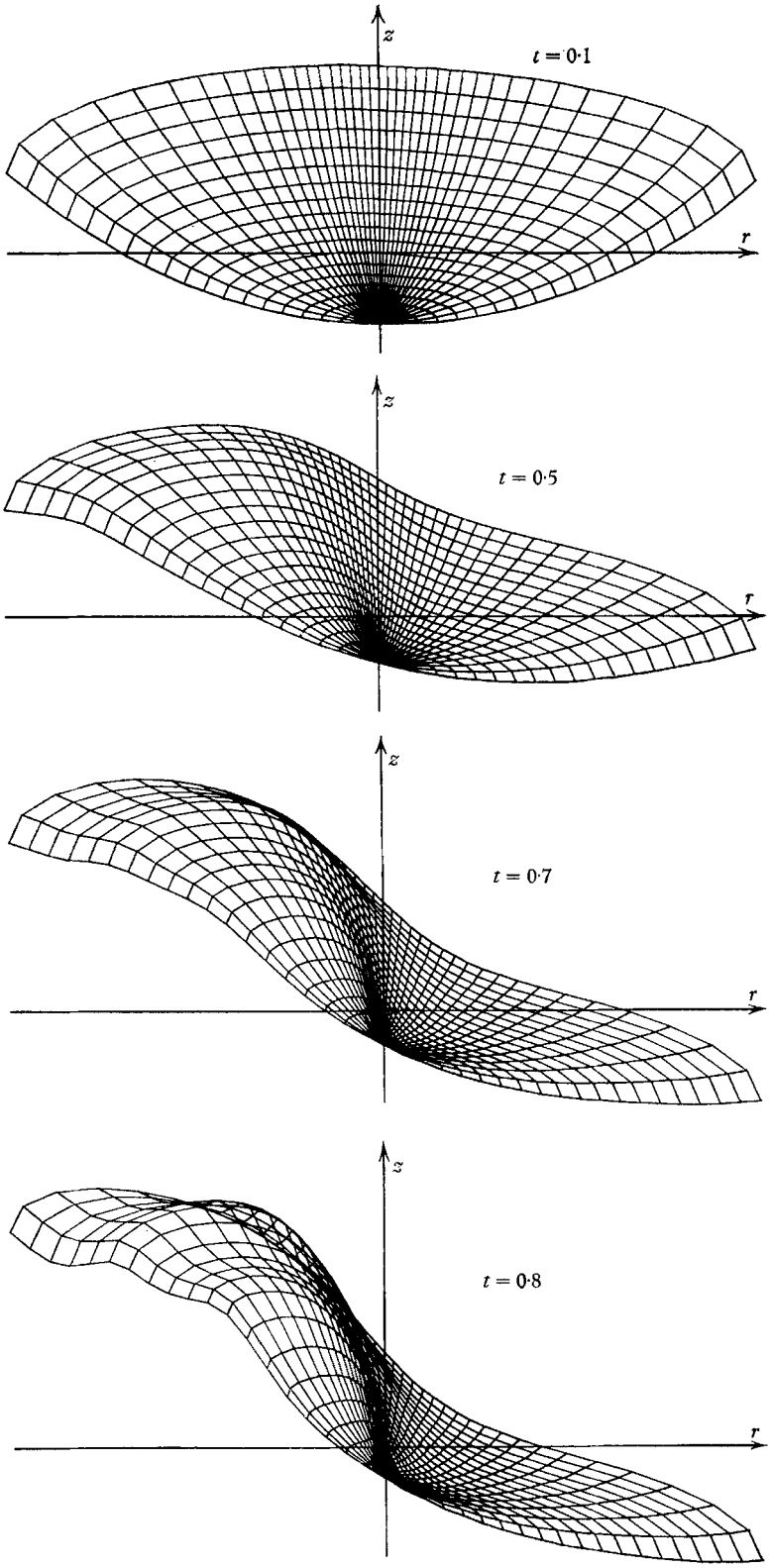

FIGURE 13. Asymmetric surface motion with $\alpha_1 = \alpha_3 = -1{\cdot}0$, $\beta = 0$, $\psi_0 = 45°$.

REFERENCES

ABRAMSON, H. N., CHU, W. H. & KANA, D. D. 1966 Some studies of nonlinear lateral sloshing in rigid containers. *J. Appl. Mech.* **33**, 774–84.

BELLMAN, R. & PENNINGTON, R. H. 1954 Effects of surface tension and viscosity on Taylor instability. *Q. Appl. Math.* **12**, 151–62.

BOWMAN, T. E. 1966 Dynamics of an axi-symmetric liquid free surface following a stepwise acceleration change. *Inst. Environmental Sci. Annual Meeting Proc.*

BUSSINGER, P. & GOLUB, G. 1965 Linear least squares solutions by Householder transformations. *Numerische Math.* **7**, 269.

CONCUS, P., CRANE, G. E. & PERKO, L. M. 1965 Inviscid fluid flow in an accelerating axisymmetric container. *Fluid Mech., and Heat Transfer Under Low-G Symp. Proc., Palo Alto, California.*

DAVIS, P. J. & RABINOWITZ, P. 1961 Advances in orthonormalizing computation. In *Advances in Computers*, volume 2. New York: Academic Press.

FUNG, F. C. W. 1965 Dynamic response of liquids in partially filled containers suddenly experiencing weightlessness. *Fluid Mech. and Heat Transfer Under Low-G Symp. Proc., Palo Alto, California.*

HARLOW, F. H. & WELCH, J. E. 1965 Numerical calculation of time dependent viscous incompressible flow of a fluid with a free surface. *Phys. Fluids*, **8**, 2182–9.

HARLOW, F. H. & WELCH, J. E. 1966 Numerical study of large amplitude free surface motions. *Phys. Fluids*, **9**, 842–51.

HOUSEHOLDER, A. S. 1958 Unitary triangularization of a nonsymmetric matrix. *J. Assoc. Comp. Mach.* **5**, 339–42.

LANDAU, L. D. & LIFSHITZ, E. M. 1959 *Fluid Mechanics*. London: Permagon Press.

LEWIS, D. J. 1950 The instability of liquid surfaces in a direction perpendicular to their planes. II. *Proc. Roy. Soc.* A **202**, 81.

MOORE, R. E. & PERKO, L. M. 1965 Inviscid fluid flow in an accelerating cylindrical containers. *J. Fluid Mech.* **22**, 305–20.

PENNY, W. G. & PRICE, A. T. 1952 Some gravity wave problems in the motion of perfect liquids. II. Finite periodic stationary gravity waves in a perfect liquid. *Phil. Trans.* A **244**, 254–68.

SATTERLEE, H. M. & REYNOLDS, W. C. 1964 The dynamics of the free liquid surface in cylindrical containers under strong capillary and weak gravity conditions. *Technical Report* LG-2, Stanford University.

SATTERLEE, H. M., HOLLISTER, M. P., PERKO, L. M. *et al.* 1967 A study of liquid propellant behaviour during periods of varying acceleration. *NASA MSFC Contract NAS-9-5174, LMSC Report A* 874728.

TAYLOR, G. I. 1950 The instability of liquid surfaces when accelerated in a direction perpendicular to their planes. *Proc. Roy. Soc.* A **201**, 192–6.

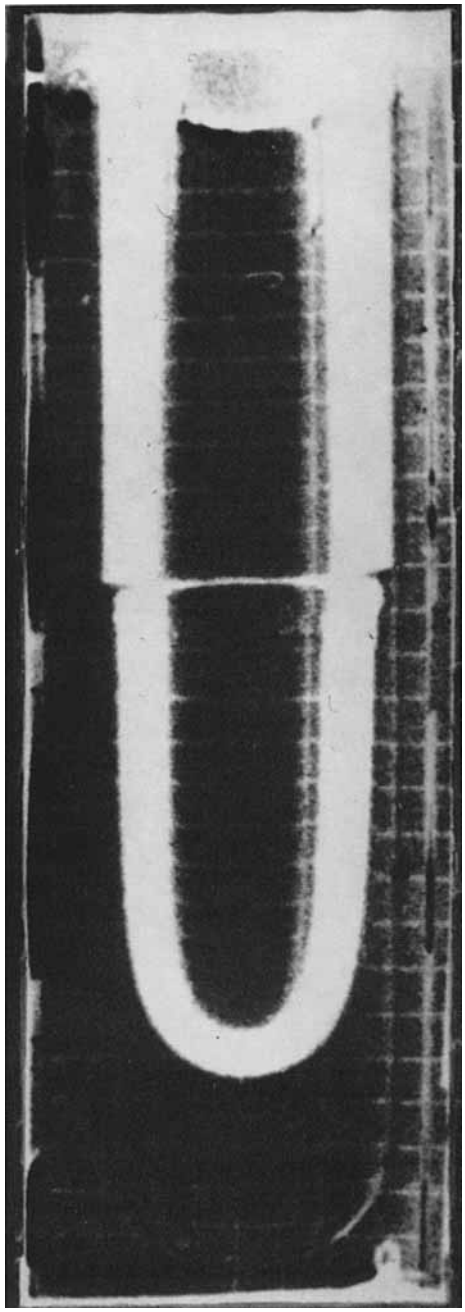

FIGURE 9. A photograph taken during the symmetric reorientation described in figure 8 corresponding to $t = 1{\cdot}55$.